Fischer, S., Liebscher, A., Wandrey, M., CO2SINK Group (2010) : CO2-brine-rock interaction – First results from long-term exposure experiments at in situ P-T conditions of the Ketzin CO2 reservoir. - Chemie der Erde - Geochemistry, 70, Suppl. 3, 155-164

DOI: 10.1016/j.chemer.2010.06.001

CO_2-Brine-Rock Interaction – First Results of Long-Term Exposure Experiments at in situ P-T Conditions of the Ketzin CO_2 Reservoir

Sebastian Fischer[1,2,*], Axel Liebscher[1], Maren Wandrey[1], and the CO_2SINK Group

[1] GFZ German Research Centre for Geosciences, Centre for CO_2 Storage, Telegrafenberg, D-14473 Potsdam, Germany
[2] Technical University of Berlin, Section Mineralogy and Petrology, Ackerstraße 76, D-13355 Berlin, Germany
[*] Corresponding author, Tel.: +49 331 / 288 28 37, Email: fischer@gfz-potsdam.de

Keywords: long-term CO_2 experiments, geochemical changes, reservoir sandstone, Stuttgart Formation, Ketzin

Abstract

Sandstone samples of the Stuttgart Formation at Ketzin have been experimentally treated with CO_2 and synthetic reservoir brine in high-quality steel autoclaves at simulated in situ P-T conditions (5.5 MPa, 40 °C). In order to observe mineralogical changes induced by CO_2, untreated samples are compared to CO_2-treated ones. Most samples show an analogous petrography of mainly quartz and plagioclase. Heterogeneities are related to minor mineral phases, such as K-feldspar, hematite, muscovite, biotite, illite, chlorite, and opaque phase(s). These are attributed to the variability of the fluvial reservoir sandstone. The samples are weakly consolidated. Analcime, dolomite and anhydrite are only found as cement phases. During the experiments dissolution of anhydrite and plagioclase is observed. SEM micrographs of CO_2-treated samples show corrosion textures on mineral surfaces of intermediate plagioclase, as well as precipitation of euhedral albite crystals. Overall, the data indicate preferred dissolution of calcium-rich plagioclase, K-feldspar and anhydrite, and stabilization or precipitation of albite.

1. Introduction

Capture and subsequent geological storage of CO_2 is a key strategy within the portfolio of actions to reduce CO_2 emissions to the atmosphere. Deep saline aquifers are the most promising geological storage options on the regional to global scale based on their estimated storage capacities and their widespread distribution. For these deep saline aquifer systems, initial physico-chemical equilibrium between saline formation fluid and reservoir rock can be reasonably assumed. However, the injection of CO_2 into these saline aquifer systems disturbs this initial equilibrium and will trigger chemical interactions between injected CO_2, saline formation fluid and reservoir rock. These interactions include dissolution of certain minerals and precipitation of others and not only change the chemical, but also the physical properties of the reservoir system. The chemical interactions may lead to mobilization of certain, eventually harmful or toxic, elements while the changes in physical properties influence injectivity, storage capacity, as well as long-term safety and stability of the reservoir. Precise knowledge of the CO_2-induced interactions between injected CO_2, saline formation fluid and reservoir rocks and of the resulting changes in chemical and physical properties of the reservoir system is therefore a prerequisite for any secure operation of a storage site. Unfortunately, due to the general lack of core samples from reservoir systems after onset of CO_2 injection, any information on CO_2-induced interactions at real storage sites are, at least up to now, indirect and mostly based on gas or fluid samples recovered from observation wells (e.g., Assayag et al., 2009). Experimental studies at simulated reservoir pressure and temperature conditions are an important and elegant way to overcome this problem. Such studies either focus on individual minerals (e.g., Daval et al., 2009; Hangx and Spiers, 2009) or on real reservoir rock samples (e.g., Kaszuba et al., 2003, 2005; Wigand et al., 2008). Kaszuba et al. (2003) studied CO_2-brine-arkose interactions during 139 days exposure experiments at 20 MPa and 200 °C. In these experiments, etch textures indicate dissolution of

microcline, biotite and quartz. In addition, smectite and magnesite precipitated. In another experimental study at 20 MPa/200 °C and 77 days run duration, Kaszuba et al. (2005) observed dissolution of biotite and shale and concomitantly increasing concentrations of magnesium, iron and manganese in the brine. In these experiments, analcime crystallized during the run and lowered the sodium concentration of the brine. In batch CO_2-exposure experiments on Bunter Sandstone at 30 MPa/60 °C and 63 days run duration, Wigand et al. (2008) discovered dissolution of dolomite cement and etch textures on K-feldspar and albite; montmorillonite precipitated in cleavages of albite crystals. Given the vast mineralogical, chemical and physical diversity of the different saline aquifer systems that may serve as potential storage sites, the number of experimental studies is, however, relatively small and the existing data base is insufficient to yield a conclusive picture of CO_2 induced interactions between injected CO_2, saline formation fluid and reservoir rocks for any specific storage site. This is especially true if one considers the low pressure and temperature conditions and therefore potentially sluggish reaction kinetics of the experiments in combination with the comparably short run durations. Further experimental studies that cover additional physico-chemical conditions (e.g., pressure, temperature, lithology, brine compositions), refer to specific geological environments at individual storage sites, and address the problem of potential sluggish reaction kinetics by prolongated run durations are therefore urgently needed.

In order to add further data to the existing data base and to specifically address the CO_2-induced interactions at the pilot storage site at Ketzin, Brandenburg (Germany), we here present first results from long-term (15 months) CO_2-exposure experiments on core samples from the Ketzin reservoir rocks. The integrative strategy of these experiments was to jointly study the mineralogical, chemical, petrophysical as well as microbiological changes of the

Ketzin reservoir rocks as induced by CO_2 on an identical set of samples. The petrophysical results are presented by Zemke et al. (2010), and the microbiological results in Wandrey et al. (2010a). In this contribution we focus on the observed mineralogical and chemical changes. We will show that although the mineralogical changes are only minor, the data provide clear evidence for preferred dissolution of certain minerals, e.g., plagioclase, with concomitant mobilization of calcium in the saline fluid.

1.1 The Ketzin pilot site

The pilot storage site at Ketzin, Brandenburg (Germany), is situated in the Northeast German Basin about 40 km west of Berlin. It is located on the south-eastern flank of the gently dipping Roskow-Ketzin double anticline, which formed above a west-east elongated salt pillow. A detailed description of the local geology is given in Förster et al. (2010) and Norden et al. (2010). The Ketzin locality is the first European on-shore CO_2 storage site in a saline aquifer. In summer 2007, one injection well (Ktzi 201) and two observation wells (Ktzi 200 and 202) had been drilled to depths of 750 to 800 m. The wells are about 50 and 110 m away from each other and are arranged in a triangular shape (Schilling et al., 2009). Since June 2008, food-grade CO_2 with a purity of > 99.9 vol% is injected into sandstone horizons of the Triassic Middle Keuper Stuttgart Formation on the south-eastern flank of the anticline. At Ketzin, the Stuttgart Formation has an average thickness of 75 to 80 m, while the main reservoir horizon is only 9 to 20 m thick (Norden et al., 2010). The Stuttgart Formation was deposited in a fluvial system, in which the sandstone horizons represent river channel deposits. This depositional environment causes a high lateral and vertical heterogeneity between, but also within the individual sandstone horizons (Förster et al., 2010). The sandstones are typically fine-grained with a general modal composition of 35 to 39 % quartz, ~ 20 % feldspar, 13 to 18 % illite, ~ 5 % analcime, up to 10 % anhydrite, plus minor but

variable amounts of mica, dolomite, hematite, pyrite, chlorite; their porosity varies between 5 and > 35 %, and their permeability is between 0.02 to > 5000 mD (Norden et al., 2010). The reservoir horizon is located at 625 to 650 m depth, and the initial reservoir conditions were ~ 33 °C/6.2 MPa, which increased to ~ 33 °C/7.5 MPa during ongoing injection of CO_2. The actual reservoir conditions correspond to a CO_2 density of ~ 0.3 g/cm^3 (Span and Wagner, 1996), which is notably less than the CO_2 density of ~ 0.8 g/cm^3 targeted for future industrial-scale storage sites.

2. Materials & Methods

2.1 Sample Description

The studied core samples were recovered from observation well Ktzi 202. The coring was performed through the uppermost 18 m of the Stuttgart Formation to a maximum depth of 635.0 m (Norden et al., 2010). Five core sections, each 1 m in length, have been sampled from depths between 627.7 (B2-2) to 634.6 m (B4-2) (Fig. 1a, Tab. 1). Of these five core sections, a total of 14 individual samples (intact core pieces between 10 to 15 cm in length and 5 cm in diameter, but also cm-sized broken fragments; Fig. 1a) were selected for the present study and split into two subsets; subset 1 (untreated) was used to describe the initial mineralogy of core sections prior to the CO_2-experiments, and subset 2 (CO_2-treated) was used for the long-term experiments. Wherever possible, attention was paid to ensure that for each core section the different samples for subset 1 and 2 were taken in close proximity to each other to minimize any initial heterogeneity between the samples and to allow for comparison between the two subsets. Nevertheless, a certain heterogeneity between the different samples is apparent in hand specimen (Fig. 1a). Most samples are finely laminated on mm- to cm-scale. This lamination predominantly appears as alternating red-brown and dark-brown colors and is due

to different grain sizes (more sandy versus more silty) next to slightly distinct modal quantities of especially clay minerals. Some samples exhibit a fine cross-bedding. Overall, the samples are only weakly consolidated and show a patchy distribution of cement, visible as uneven spread mm-sized brighter parts.

2.2 Experimental Procedure

For 15 months, the samples from subset 2 were stored together with synthetic reservoir brine and pure CO_2 in high-quality steel pressure vessels that were placed in a heating cabinet at simulated reservoir conditions of 5.5 MPa and 40 °C. The synthetic reservoir brine had an initial composition of 172.8 g/l NaCl, 8.0 g/l $MgCl_2*6H_2O$, 4.8 g/l $CaCl_2*2H_2O$, and 0.6 g/l KCl according to data on the original Ketzin formation fluid available at the start of the experiments (Förster et al., 2006). Subsequent studies on the original Ketzin formation fluid showed that the synthetic brine unfortunately contains only about 81 % of the total dissolved solids (TDS) of the original formation fluid and lacks any sulphate (Wandrey et al., 2010b). Therefore, some mineral reactions are expected, which may not related to the presence of CO_2.

2.3 Analytical Techniques & Methods

After the samples were taken out of the autoclaves they have been washed several times with pure H_2O and cautiously dried in a compartment drier at 45 °C. The samples were embedded in blue colored epoxy resin to enforce stability for sawing and thin section preparation. Thin sections are oriented perpendicular to the bedding planes and were prepared at the Section of Mineralogy at the Technical University of Berlin (TUB). A Leitz polarizing microscope was used for thin section analyses and to take micrographs. The grain size of each sample was

measured on the average long-axes of 50 grains per sample using a software tool kit. Roundness and sorting were determined by standard charts for comparison (Pettijohn et al., 1987).

Powder specimens for X-ray diffraction analyses (XRD) with Rietveld refinement were obtained from each sample to determine the modal mineralogy. These powders were first homogenized in an agate mortar for a few minutes and then evenly spread on a circular foil. The XRD measurements were carried out at the TUB on a Phillips PW1050 with a Seifert Iso-Dedyeflex generator (40 kV, 20 mA) and a fixed divergence slit, as well as on a Phillips PW1050 with a Phillips PW1729 generator (40 kV, 30 mA) and an automatic divergence slit. Powder X-ray diffractograms were recorded between 5-80 ° 2-Theta with Cu-Kα cross ($\alpha_{1,2}$) = 1.5419 Å. The detector step size was set to 0.02 with 2 sec/step. Electron Microprobe (EMP) analyses was performed on a Cameca SX 100 at the GFZ. Accelerating voltage was 15 kV, beam current was 20 nA. The beam diameter was 5 µm for mica, 20 µm for carbonate, and 10 µm for feldspar and all other minerals. Scanning electron microscopy (SEM) was done on a Zeiss ultra 55 plus at the GFZ. The SEM operated at 20 kV and 15 nA and is equipped with an energy dispersive X-ray system (EDS). Analyses were done on small sample pieces. Backscattered electron (BSE) images were taken on polished thin sections also used for EMP measurements.

3. Results

3.1 Petrography

In thin section, the analyzed samples are mainly fine grained (<200 µm), moderately well- to well sorted, angular to subangular and only partly consolidated sandstones. The principal modal mineral composition as determined by optical microscopy, XRD measurements, EMP

and SEM analyses is comparable between all samples (Tab. 1, Figs. 2 and 3). They are mainly composed of quartz and plagioclase; K-feldspar, mica, hematite, clay minerals, opaque phase(s), and lithoclasts are present in subordinate and varying amounts. Mica is predominantly muscovite with only minor amounts of biotite. Chlorite and illite are the most important clay minerals, which are often associated with lithoclasts. These lithoclasts are predominantly composed of either quartz and sheet silicates or comprise feldspar with quartz, opaque phase(s), chlorite, and illite. These observations are in good accordance with the results by Förster et al. (2010). The samples are weakly cemented by anhydrite, analcime, and/or dolomite. The cements form unevenly distributed, isolated, poikilitic patches (Fig. 2a, b and d). Anhydrite and analcime are present in all untreated samples. In the CO_2-treated samples, however, anhydrite was not observed in samples from core sections B3-1, B3-3, and B4-2 and analcime does not occur in samples from core section B4-2. Dolomite is only present in both untreated and CO_2-treated samples from core sections B2-2 and B2-3. With the exception of anhydrite and analcime being absent in some of the CO_2-treated samples, the mineralogical variability between samples from subset 1 is larger than that between untreated and CO_2-treated samples from identical core sections.

The heterogeneity and lamination of the samples observed in hand-specimen is also apparent on the thin-section scale. Here, these heterogeneities are mostly caused by an uneven distribution of minor mineral phases like hematite, chlorite, illite, and of the cement phases. The lamination is caused by alternation of lighter, quartz- and feldspar-dominated layers with darker, (red-)brownish to black layers, which are mainly composed of opaque phase(s) with notably less quartz, feldspars and cements. In some samples, these darker domains cover relatively large and interconnected areas, while in others they occur in only scattered and elongated zones. In close vicinity to the dark layers, mineral grains with thin rims (coatings) are more frequent. These coatings were already described as iron(-titanium)-(hydr)oxides by

Förster et al. (2010); own EMP analyses suggest mostly hematite. According to the measurements by Zemke et al. (2010), the initial porosity of the samples varies between 20 and 30 %.

3.2 Mineral Surfaces

Mineral surfaces of quartz are generally clean and smooth without any signs of alteration (Fig. 4a). Micas show platy morphology with the typical basal cleavage and, like quartz, lack any signs of alteration (Fig. 4b). Anhydrite typically shows good cleavages in three directions. Despite the fact that anhydrite was not found in the CO_2-treated samples from three core sections (see above), which suggest dissolution of anhydrite, individual anhydrite crystals do not show any clear evidence of dissolution (Fig. 4c). Only plagioclase crystals show unambiguous evidence of alteration and dissolution. Plagioclase grains typically show either surfaces with crystallographically oriented etch textures (Fig. 4d) or lamellar dissolution features resulting in a lumpy and irregular surface morphology (Fig. 4e). Comparable dissolution textures are occasionally found in K-feldspar grains. However, here these textures are not that distinct. At times, pure albite grains may show absolutely clean and fresh euhedral crystal habit (Fig. 4f). These albite grains are, however, only found in the CO_2-treated samples and may have precipitated during the experiments.

3.3 Mineral Composition

3.3.1 Feldspar

The feldspar composition before and after the experiment is shown in Figure 5, and representative feldspar analyses are given in Table 2a and b. No major compositional changes

during the experiments are obvious. Plagioclase measurements show clusters with two different compositions: intermediate compositions have Ab_{40} to Ab_{80} with $Or_{<10}$, while albite rich compositions have $Ab_{>95}$. Maximum calcium contents in plagioclase are An_{59} in untreated and An_{55} in CO_2-treated samples. K-feldspar from untreated and CO_2-treated samples consistently ranges from Or_{70} to Or_{98}. Only very few measurements plot at intermediate alkali feldspar composition or in the compositional field of true ternary feldspars. These may reflect inaccuracies or measurements of mixed mineral phases. Despite the overall consistency of the feldspar composition before and after the experiments, the plagioclase composition indicates changes. Much more sodium-rich to pure albite grains have been measured in CO_2-treated samples compared to the untreated ones. Even more, pure albite ($Ab_{>99}$) was only found in the CO_2-treated samples. In combination with the petrographical observations (see above), this also indicates precipitation of pure albite during the experiments.

3.3.2 Sheet silicates

Representative analyses of sheet silicates are given in Table 3a. As for feldspar, no major changes in chemical composition during the experiments are obvious. White mica is predominantly muscovite; only one analysis showed paragonite. Octahedral aluminum in muscovite ranges from 1.43 to 1.92 cation per formula unit (pfu), other octahedral cations are 0.04 to 0.39 iron pfu, 0.04 to 0.38 magnesium pfu and 0.01 to 0.17 titanium pfu. Potassium contents on the XII-fold coordinated A-site range from 0.46 to 0.96 pfu, and sodium concentrations are between 0.02 and 0.42 pfu. Dark mica is biotite of the phlogopite-annite solid solution series. Octahedral iron content ranges from 0.88 to 1.56 pfu, while magnesium is 0.70 to 1.34 pfu. Titanium contents are between 0.09 and 0.25 pfu, and octahedral aluminum is 0.04 to 0.56 pfu. In biotite, the XII-fold coordinated A-site is exclusively

occupied by potassium (0.58 to 0.96 pfu); A-site vacancies, i.e. a talc component, reach a maximum of 0.40 pfu. Biotite analyses from untreated samples of core sections B2-2 and B3-1 yield very low totals of < 90 wt% oxides (not shown in Table 3) and may indicate notable chloritization of biotite in these samples. EMP analyses of chlorite indicate compositions of the chlinochlore-chamosite solid solution series.

3.3.3 Cement phases

All three cement phases anhydrite, analcime and dolomite consistently show stoichiometrical compositions before and after the experiments and provide no hints for any chemical alteration. Anhydrite forms relatively coarse (poikilitic) grains (Fig. 2 a-d), but a chemical zoning, with respect to calcium and strontium as described by Förster et al. (2010), was not observed. Analcime has near end-member composition and forms smaller crystals that appear to be very homogenous and optically clear (Fig. 2d). Dolomite cement occurs as isolated, blocky patches (Fig. 2a and b) and has a very uniform composition of calcium and magnesium both approximately accounting for 0.50 pfu. Only traces of iron and manganese were detectable. These little concentrations are likely to be the reason for the shaded appearance observable in the BSE images of Figure 2a and b.

4. Discussion

The presented data only show minor mineralogical changes during the experiments. The variability between comparable samples before and after the experiments is lower than the overall variability of the studied samples and no significant changes in mineralogy were observed. Nevertheless, several lines of evidence indicate chemical interactions between CO_2, brine and sandstone samples during the experiments. The presence of anhydrite in all

untreated samples, but its absence in CO_2-treated samples from core sections B3-1, B3-3, and B4-2 is at least indicative of anhydrite dissolution. The distinct corrosion and etch textures on plagioclase surfaces, and also on K-feldspar surfaces clearly indicate preferred dissolution of these minerals. On the other hand, euhedral albite grains occurring in CO_2-treated samples suggest precipitation of albite, most likely in expense of plagioclase, during the experiments. Dissolution of certain minerals is consistent with results from porosity measurements on the same samples (Zemke et al., 2010). These measurements generally indicate a slight increase in porosity during the experiments and also imply dissolution processes. Preferred dissolution of anhydrite and of the anorthite component of plagioclase should also increase the calcium and sulfate concentrations in the brine, as long as no other calcium- and/or sulphate-bearing minerals precipitate. Again, this is consistent with first data on the composition of the synthetic brine. After 15 months, the calcium and sulfate (but also potassium and magnesium) concentrations in the brine have notably increased (Wandrey et al. 2010a). As the initial concentrations of calcium and sulfate in the synthetic brine were below those of the Ketzin formation fluid (see above), one may argue that this increase in concentration simply reflects the evolution of the synthetic brine to its potential equilibrium composition, without any influence of CO_2. However, the measured concentrations of calcium, potassium, and magnesium in the brine after the experiments are notably higher than those of the original Ketzin formation fluid. Accordingly, these cannot only be explained by the above mentioned attainment of equilibrium without any influence of CO_2. Overall, the data presented in this paper in combination with those given by Wandrey et al. (2010a and b), as well as Zemke et al. (2010) clearly indicate that the addition of CO_2 triggered preferred dissolution of the anorthite component of plagioclase, dissolution of K-feldspar and anhydrite, and precipitation of pure albite.

The indicated corrosion effects are observable in SEM micrographs, in which the plagioclase crystals display heavily altered edges with holes, etched pits and lamellae. These features were not observed – at least not to that degree – in the untreated samples and thus suggest intensified alteration processes during the experiments triggered by CO_2. But as Bertier et al. (2006) also discussed, it is generally difficult to quantify alterations of alumosilicates (e.g feldspars), when pre-experimental, diagenetic alterations of these minerals exist. In contrast to that, fresh and unaltered euhedral albite grains in some of the CO_2-treated samples (Fig. 4f) clearly suggest equilibrium between albite and the brine-CO_2 fluid. Because the feldspar composition observed in EMP analyses shows preferred occurrence of pure albite minerals after the CO_2-treatment, it is reasonable to assume precipitation of these euhedral albite grains during the experiments. But Förster et al. (2010) also determined albite end-member compositions as a result of diagenetic albitization of both plagioclase and K-feldspar. On the other hand, Bertier et al. (2006) likewise observed new formed albite minerals during lab-experiments. Still it is possible that the higher number of albite measurements after the experiments are owed to the natural variability of the reservoir system, possibly displaying some statistical artifacts. Independent of CO_2-exposure lab-experiments, Blum & Stillings (1995) reported that in acidic environments, feldspar weathering rates are generally higher for calcic plagioclase compared to sodic plagioclase. And also Deer et al. (1992) stated that during hydrothermal plagioclase alteration, sodic varieties are more stable than those richer in the anorthite component. This kinetic mechanism is related to the structure of albite and anorthite. While an extensive framework of linked silicate tetrahedra, which are resistant to hydrolysis relative to aluminate sites, characterize the structure of albite, in anorthite, on the contrary, silicate tetrahedra are isolated from one another by aluminate groups so that selective hydrolysis (of aluminium) completely disrupts the anorthite structure (Casey et al, 1991), respectively. Parallel to this statement, Sass et al. (1999) debated that calcium was partially replaced by sodium in feldspar reactions occurring during the interaction of rock

minerals (feldspar and clay) with CO_2 and brine. Shmulovich and Graham (2008) concluded that an increase in the bulk salinity of the fluid stimulates reactions in which alkali earth cations (e.g. calcium) are substituted for alkalis (e.g. sodium).

While quartz does not show any signs of dissolution, K-feldspars also seems to be partly dissolved during the CO_2-treatment. Comparable to plagioclase but less frequent, some K-feldspar grains in CO_2-treated samples show corrosion textures (Fig. 2c). Yet it is hardly possible to differentiate diagenetic and experimental, CO_2 induced alteration processes (see above). Similar alterations of K-feldspar during CO_2-exposure experiments have also been reported by Parry et al. (2007).

Although mica minerals do not occur in large quantity, they are an important component of the reservoir and complete the understanding of the reservoir system behavior. Additionally, alterations of mica minerals could easily lead to the formation of clay minerals, such as kaolinite, illite, and chlorite, which may have an impact on petrophysical properties of the reservoir. These authigenic clays could clog pore throats and fill open cleavages to reduce poroperm levels and in turn hamper the injection of CO_2. Precipitation of smectite, intergrown with magnesite on biotite has already been reported by Kaszuba et al. (2003). Shiraki and Dunn (2000) presumed that a permeability decrease due to the formation of clay minerals could be a characteristical feature of CO_2 storage in formations containing alumosilicate minerals. On the other hand, Watson et al. (2004) concluded that reservoirs rich in feldspars and labile rock fragments, which can react with CO_2 to form new solid carbonate phases, are important for a save and successful long-term storage site. (Of course an effective poroperm level has to be assured at the same time.) In the here presented study, no unambiguous

evidence for such mica alterations or intensified clay mineral formation was found, although these are likely to occur. Only illitization of muscovite could be indicated by the lowered potassium and aluminum contents of muscovite during the runs. Förster et al. (2010) did furthermore report chloritization of detrital biotite triggered by diagenetic processes in the Stuttgart Formation.

Cements are in general a very important feature of reservoir systems because of influencing hydraulical parameters like porosity, permeability, and injectivity, which are vital for a successful site operation. Hence, they need to be carefully analysed concerning mineralogical changes, precipitation and dissolution kinetics. The discussed dissolution of anhydrite was also observed by Shiraki and Dunn (2000) during core-flooding experiments on reservoir sandstones saturated with synthetic reservoir brine and CO_2.

The increased TDS concentration in the brine due to the dissolution of plagioclase, K-feldspar (alumosilicates) and anhydrite may trigger subsequent precipitation of (carbonate phases. Such carbonate formation in different sandstones during laboratory CO_2-experiments has been described by, e.g., Czernichowski-Lauriol et al. (2006), Parry et al. (2007). Ketzer et al. (2009), and Kampman et al. (2009). However, analogous reactions have not yet been observed in the studied samples of the Stuttgart Formation but might only be a matter of time.

5. Conclusions

The petrological investigations observed by thin section analysis and XRD showed no significant mineralogical or petrochemical changes after the experiments. The variability of

the Stuttgart Formation, which is primarily attributed to the sandstone sedimentation in a meandering, fluvial environment generating the incised-valley deposition with shoe-string-like sandstone bodies, is higher than that between untreated and CO_2-treated samples. Accordingly, the natural variability of the reservoir hampers the comparability of samples before and after CO_2 exposure. The cement phases do show analogous mineralogy and no signs of alteration except dissolution of anhydrite. Corrosion textures on feldspar minerals (plagioclase and K-feldspar) indicate alteration processes, while euhedral albite crystals suggest stabilization or even precipitation. The increased number of pure albite grains indicates albitization alongside preferred anorthite dissolution. Based on our data, the integrity of the reservoir formation at Ketzin is not affected by CO_2.

Acknowledgements

It is thankfully acknowledged that Christa Zecha did the preparation of the thin sections at the TUB. We also thank Christa Kotré of the Section of Mineralogy and Petrology at the TUB for doing the XRD measurements and for assisting in preliminary data conditioning. Oona Appelt was very helpful by introducing the EMP device and by assisting during the measurements at the GFZ. Gabriele Arnold and Juliane Herwig from the GFZ helped to prepare the core fragments for SEM analyses and to operate the SEM device. We owe them the excellent micrographs. Thank you.

This study is funded by the Federal Ministry of Education and Research (BMBF) through the GeoEnergy (GeoEn) project.

6. References

Assayag, N., Matter, J., Ader, M., Goldberg, D., and Agrinier, P., 2009. Water-rock interactions during a CO_2 injection field-test: implications on host rock dissolution and alteration effects. Chem Geol, 265, 227-235.

Bertier, P., Swennen, R., Laenen, B., Lagrou, D., and Dreesen, R., 2006. Experimental identification of CO_2-water-rock interactions caused by sequestration of CO_2 in Westphalian and Buntsandstein sandstones of the Campine Basin (NE Beldium). J. Geochem. Explor., 89, 10-14.

Beutler, G., 2005. Stratigraphie von Deutschland IV – Keuper, Cour. Forsch.-Inst. Senckenberg. 253, Stuttgart.

Blaschke, A.-W., Schöner, R., Gaupp, R., and Förster, A., 2008. Sandstone petrography and pore system of the Upper Triassic Stuttgart Formation from a CO_2 pilot storage site (Ketzin, Germany). Geo2008 – Resources and Risks in the Earth System, Schriftenr. Dt. Geow. (SDGG), 60, 301.

Blum, A. E., and Stillings, L. L., 1995. Feldspar Dissolution Kinetics. In: White, A.F., and Brantley, S.L. (Eds.), Chemical Weathering Rates of Silicate Minerals, Min. Soc. Am., 31, 291-351.

Casey, W. H., Westrich, H. R., and Holdren, G. R., 1991. Dissolution rates of plagioclase at pH = 2 and 3. Am. Mineral., 76, 211-217.

Czernichowski-Lauriol, I., Rochelle, C., Gaus, I., Azaroual, M., Pearce, J., and Durst, P., 2006. Geochemical Interactions between CO_2, Pore-water and Reservoir Rock. Advances in the Geological Storage of Carbone Dioxide, 65, 157-174.

Daval, D., Martinez, I., Corvisier, J., Findling, N., Goffé, B. and Guyot, F. 2009. Carbonation of Ca-bearing silicates, the case of wollastonite: Experimental investigations and kinetic modeling. Chem. Geol., 265, 63-78.

Deer, W. A., Howie, R. A., and Zussman, J., 1992. An Introduction to the Rock-Forming Minerals (2^{nd} Edition), Prentice Hall, London.

Förster, A, Norden, B., Zinck-Jorgensen, K., Frykman, P., Kuhlenkampff, J., Spangenberg, E., Erzinger, J., Zimmer, M., Kopp, J., Borm, G., Juhlin, C., Cosma, C.-G., and Hurter, S., 2006. Baseline Characterization of the CO_2SINK Geological Storage Site at Ketzin, Germany, Environ. Geosci., 13, 3, 145-161.

Förster, A., Schöner, R., Förster, H.-J., Norden, B., Blaschke, A.-W., Luckert, J., Beutler, G, Gaupp, R., and Rhede, D., 2010. The Upper Triassic Stuttgart Formation (Middle Keuper) at Ketzin: The reservoir for pilot CO_2 storage in the Northeast German Basin. Mar. Pet. Geo., in press.

Hangx, S. J. T., and Spiers, C. J., 2009. Reaction of plagioclase feldspars with CO_2 under hydrothermal conditions. Chem. Geol., 265, 88-98.

IPCC, 2005. IPCC special report on carbon dioxide capture and storage. In: Metz, B., Davidson, O., de Coninck, H. C., Loos, M., Meyer, L. A. (Eds.), Prepared by Working Group III of the Intergovernmental Panel on Climate Change. Cambridge University Press, Cambridge, UK/New York.

Kampman, N., Bickle, M., Becker, J., Assayag, N., and Chapman, H., 2009. Feldspar dissolution kinetics and Gibbs free energy dependence in a CO_2-enriched groundwater system, Green River, Utah. Earth Planel. Sci. Lett., 284, 473-488.

Kaszuba, J. P., Janecky, D. R., and Snow, M. G., 2003. Carbon dioxide reaction processes in a modal brine aquifer at 200 °C and 200 bars: implications for geological sequestration of carbon. Appl. Geochem., 18, 1065-1080.

Kaszuba, J. P., Janecky, D. R., and Snow, M. G., 2005. Experimental Evaluation of Mixed Reactions between Supercritical Carbon Dioxide and NaCl Brine: Relevance to the Integrity of a Geologic Carbon Repository. Chem. Geol., 217, 277-293.

Ketzer, J. M., Iglesias, R., Einloft, S., Dullius, J., Ligabue, R., and de Lima, V., 2009. Water–rock–CO_2 interactions in saline aquifers aimed for carbon dioxide storage: Experimental and numerical modeling studies of the Rio Bonito Formation (Permian), southern Brazil. Appl. Geochem., 24, 5, 760-767.

Kretz, R.,1983. Symbols for Rock-forming Minerals. Am. Mineral., 68, 277-279.

Norden, B., Förster, A., Vu-Hoang, D., Marcelis, F., Springer, N., and Le Nir, I., 2010. Lithological and petrophysical core-log interpretation in the CO_2SINK, the European CO_2 onshore research storage and verification project. SPE Reservoir Evaluation & Engineering, 13, 2, 179-192.

Parry, W. T., Forster, C. B., Evans, J. P., Bowen, B. B., and Chan, M. A., 2007. Geochemistry of CO_2 Sequestration in the Jurassic Navajo Sandstone, Colorado Plateau, Utah. Environ. Geosci., 14, 2, 91-109.

Pettijohn, F.J., Potter, P. E., Siever, R., 1987. Sand and Sandstones. Springer, New York.

Sass, B. M., Gupta, N., Ickes, J. A., Engelhard, M. H., Baer, D. R., Bergman, P., Byrer, C., 1999. Interaction of Rock Minerals with Carbon Dioxide and Brine: A Hydrothermal Investigation. In: Conference Proceedings CD, 1st National Conference on Carbon Sequestration, Washington, DC.

Schilling, F., Borm, G., Würdemann, H., Möller, F., Kühn, M., and the CO_2SINK Group, 2009. Status Report on the First European on-shore CO_2 Storage Site at Ketzin (Germany). Energy Procedia, 1, 1, 2029-2035.

Shiraki, R., and Dunn, T. L., 2000. Experimental study on water-rock interactions during CO_2 flooding in the Tensleep Formation, Wyoming, USA. Appl. Geochem., 15, 265-279.

Shmulovich, K. I., and Graham, C., 2008. Plagioclase-Aqueous Solution Equilibrium: Concentration Dependence. Petrology, 16, 2, 177-192.

Wandrey, M., Fischer, S., Zemke, K., Liebscher, A., Scherf, A.-K., Vieth, A., Zettlitzer, M., and Würdemann, H., 2010a. Monitoring petrophysical, mineralogical, geochemical and microbiological effects of CO_2 exposure – Results of long-term experiments under *in situ* condition. GHGT 10, Amsterdam, accepted.

Wandrey, M., Morozova, D., Zettlitzer, M., Würdemann, H., and the CO_2SINK Group, 2010b. Assessing drilling mud and technical fluid contamination in reservoir rock and brine samples from the Ketzin storage site using fluorescent dye tracers. Int. J. Greenhouse Gas Control, in press.

Watson, M. N., Zwingmann, N., and Lemon, N., 2004. The Ladbroke Grove-Katnook Carbon Dioxide Natural Laboratory: A Recent CO_2 Accumulation in a Lithic Sandstone Reservoir. Energy, 29, 9-10, 1457-1466.

Wigand, M., Carey, J.W., Schütt, H., Spangenberg, E., and Erzinger, J., 2008. Geochemical Effects of CO_2 sequestration in sandstones under simulated in situ conditions of deep saline aquifers. Appl. Geochem., 23, 2735-2745.

Zemke, K., Liebscher, A., Wandrey, M., and the CO_2SINK Group, 2010. Petrophysical analysis to investigate the effects of carbon dioxide storage in a subsurface saline aquifer at Ketzin, Germany (CO_2SINK). Int. J. Greenhouse Gas Control, in press.

Figure captions

Figure 1: (a) Profile of the Stuttgart Formation in observation well Ktzi 202, modified after Förster et al. (2010). Shown is the depth interval of the saline aquifer sandstone next to the positions of the different samples. Photographs of the different samples (cores and rock fragment) optically visualizing the internal heterogeneities of samples. (b) Schematic sketch of the experimental setup. Not shown is the heating cabinet, which controls the temperature.

Figure 2: BSE images of polished thin sections. Labeled are the major mineral phases; black colour represents pore space. (a) Sandstone cemented anhydrite and dolomite in the untreated sample B2-2. The arrows in (b) shows marginal alteration of a plagioclase grain in the CO_2-treated sample B2-3. (c) Dissolution of K-feldspar grain (arrow). (d) Patchy pore-filling anhydrite and analcime. The latter two images (c & d) are taken from CO_2-treated sample B2-2.
Abbreviations after Kretz (1983); Frag = rock fragments, Fe = iron-(hydr)oxide.

Figure 3: Representative XRD diffractograms comparing the modal mineralogy of the twin sample B3-1. It is apparent that not only the peak positions, but also the intensities [counts] are similar for untreated (top) and CO_2-treated (bottom) measurements.

Figure 4: SEM images taken on freshly broken fragments displaying the characteristical appearance of quartz (a & b), muscovite (b), and anhydrite (c). Corrosion textures on surfaces and edges of plagioclase grains are apparent in d & e. (f) Euhedral albite crystal.

Figure 5: EMP data displaying the feldspar chemistry of untreated (open circles) and CO_2-treated samples (filled circle). While no changes are indicated for K-feldspars, much more albite minerals occur in the CO_2-treated samples.

Tab. 1: Summary of the studied samples and their basic mineralogy determined by thin section, XRD and EMP analyses.

Sample		B 2-2		B 2-3		B 3-1		B 3-3		B 4-2	
Depth [m]		627.7 - 628.7		628.7 - 629.6		629.6 - 630.6		631.6 - 632.6		633.6 - 634.6	
CO_2		untreated	treated	untreated	treated	untreated	treated	untreated	treated	untreated	treated
Qtz		+	+	+	+	+	+	+	+	+	+
Pl		+	+	+	+	+	+	+	+	+	+
Kfs		o	o	o	o	o	o	o	o	o	/
Ms		-	-	-	-	-	-	-	-	-	-
Bt		/	-	-[?]	/	/	-	/	-	-[?]	-
Cement	Anh	o	o	o	o	o	/	o	/	o	/
	Anl	o	o	o	o	o	o	o	o	o	/
	Dol	o	o	o	o	/	/	/	/	/	/
Accessory	Fe-Phase	-	-	-	-	-[a]	-[a]	-	-	-[a]	-
	Chl	/	/	-	-	-	-	-	-	-	-
	Ill										-

Categories: + = >25%, o = 5-25%, - = <5%, / = not present

Note: Mineral abbreviations after Kretz (1983); Fe-Phase: subsumes opaque phases, iron-oxides and iron-hydroxides; Ill only listed when clearly identified.

[a]: Hematite present as proven by XRD.

[?]: Biotite between 68 and 88wt.% only

Tab. 2a: Representative K-feldspar compositions determined by EMP analyses.

	B2-2		B2-3		B3-1		B3-3		B4-2	
	untreated	CO_2-treated	untreated	CO_2-treated	untreated	CO_2-treated	untreated	CO_2-treated	untreated	CO_2-treated
SiO_2	65.73	64.55	65.38	64.25	65.13	64.25	64.90	65.30	64.25	65.21
Al_2O_3	17.23	18.66	18.48	18.84	18.64	18.49	18.48	18.51	18.66	18.57
MgO	0.07	0.00	0.00	0.01	0.02	0.00	0.00	0.01	0.00	0.01
FeO	0.45	0.04	0.00	0.07	0.12	0.39	0.11	0.12	0.18	0.03
CaO	0.72	0.00	0.00	0.00	0.02	0.00	0.02	0.00	0.00	0.00
BaO	0.36	0.18	0.21	1.22	0.05	0.31	0.55	0.22	0.22	0.14
Na_2O	0.76	0.76	1.05	0.57	0.34	0.77	0.54	0.85	0.53	1.21
K_2O	14.35	15.85	15.49	15.42	16.27	15.58	15.72	15.75	16.20	15.31
∑	99.66	100.04	100.62	100.37	100.59	99.80	100.32	100.75	100.04	100.47
normalized to 8 oxygen										
Si	3.04	2.98	3.00	2.98	2.99	2.98	3.00	3.00	2.98	2.99
Al	0.94	1.02	1.00	1.03	1.01	1.01	1.01	1.00	1.02	1.00
∑	3.98	4.00	4.00	4.01	4.00	3.99	4.01	4.00	4.00	3.99
K	0.85	0.93	0.91	0.91	0.95	0.92	0.93	0.92	0.96	0.90
Ca	0.04	0.00	0.00	0.00	0.00	0.00	0.00	0.00	0.00	0.00
Na	0.07	0.07	0.09	0.05	0.03	0.07	0.05	0.08	0.05	0.11
Ba	0.01	0.00	0.00	0.02	0.00	0.01	0.01	0.00	0.00	0.00
Mg	0.00	0.00	0.00	0.00	0.00	0.00	0.00	0.00	0.00	0.00
Fe	0.02	0.00	0.00	0.00	0.00	0.02	0.00	0.00	0.01	0.00
∑	0.98	1.01	1.00	0.99	0.99	1.01	0.99	1.01	1.02	1.01
x_{kfs}	0.88	0.93	0.90	0.93	0.97	0.92	0.94	0.92	0.95	0.89
x_{an}	0.04	0.00	0.00	0.00	0.00	0.00	0.00	0.00	0.00	0.00
x_{ab}	0.07	0.07	0.09	0.05	0.03	0.07	0.05	0.08	0.05	0.11

Tab. 2b: Representative plagioclase compositions determined by EMP analyses.

	B2-2						B2-3						B3-1						B3-3						B4-2					
	untreated			CO_2-treated			untreated			CO_2-treated			untreated			CO_2-treated			untreated			CO_2-treated			untreated			CO_2-treated		
SiO_2	62.49	67.14	57.49	60.69	65.30	55.35	60.64	67.11	52.08	60.69	67.01	56.99	63.01	66.59	59.44	63.31	67.20	55.26	63.08	63.66	55.03	59.94	68.58	54.24	62.95	67.42	58.58	60.11	65.19	60.38
Al_2O_3	23.05	20.65	27.51	24.95	22.11	28.52	24.79	20.71	30.40	24.95	20.06	27.49	23.22	20.19	25.00	24.14	19.26	27.57	22.51	21.33	28.56	24.56	19.75	28.32	23.25	19.86	26.08	24.87	21.52	24.55
MgO	0.00	0.12	0.00	0.00	0.08	0.00	0.01	0.00	0.00	0.00	0.01	0.00	0.00	0.00	0.01	0.25	0.08	0.01	0.00	0.27	0.00	0.00	0.01	0.10	0.00	0.10	0.02	0.02	0.00	0.00
FeO	0.23	0.18	0.32	0.20	0.96	0.11	0.22	0.08	0.13	0.20	0.17	0.07	0.31	0.06	0.35	0.64	0.84	0.31	0.30	1.17	0.30	0.32	0.06	0.61	0.13	0.32	0.11	0.01	0.33	0.29
CaO	4.21	1.02	8.53	6.29	0.59	10.54	6.14	0.72	12.57	6.29	0.46	9.24	4.22	0.76	6.88	0.37	0.08	9.87	3.87	0.15	10.75	5.88	0.06	11.35	4.65	0.14	7.54	6.07	2.39	6.27
BaO	0.09	0.03	0.01	0.03	0.41	0.06	0.03	0.00	0.05	0.03	0.30	0.00	0.00	0.04	0.06	0.00	0.31	0.09	0.08	0.09	0.00	0.05	0.05	0.00	0.15	0.00	0.04	0.03	0.08	0.08
Na_2O	9.06	11.36	6.79	8.41	10.72	5.75	8.09	11.85	4.88	8.41	11.71	6.76	9.30	11.71	7.46	8.86	11.22	5.89	9.00	10.75	5.49	8.46	12.12	5.05	8.85	12.22	7.50	8.48	10.56	7.65
K_2O	0.92	0.11	0.18	0.19	0.00	0.20	0.89	0.05	0.08	0.19	0.01	0.03	1.06	0.03	0.59	3.13	0.02	0.52	1.10	1.03	0.35	0.50	0.00	0.26	0.75	0.06	0.51	0.27	0.25	0.92
∑	100.04	100.61	100.84	100.76	100.17	100.53	100.80	100.52	100.19	100.76	99.73	100.58	101.11	99.39	99.80	100.70	99.00	99.52	99.93	98.46	100.48	99.71	100.63	99.92	100.72	100.12	100.38	99.86	100.32	100.13
normalized to 8 oxygen																														
Si	2.78	2.93	2.56	2.69	2.87	2.48	2.69	2.93	2.36	2.69	2.95	2.55	2.78	2.94	2.67	2.80	2.98	2.51	2.81	2.87	2.48	2.69	2.98	2.46	2.78	2.96	2.62	2.68	2.87	2.70
Al	1.21	1.06	1.44	1.30	1.15	1.51	1.30	1.07	1.63	1.30	1.04	1.45	1.21	1.05	1.32	1.26	1.01	1.48	1.18	1.13	1.51	1.30	1.01	1.51	1.21	1.03	1.37	1.31	1.12	1.29
∑	3.99	3.99	4.00	3.99	4.02	3.99	3.99	4.00	3.99	3.99	3.99	4.00	3.98	3.99	3.99	4.05	3.99	3.99	3.99	4.00	3.99	3.99	3.99	3.97	3.99	3.99	3.99	3.99	3.99	3.99
K	0.05	0.01	0.01	0.01	0.05	0.01	0.05	0.00	0.00	0.01	0.01	0.00	0.06	0.00	0.03	0.18	0.05	0.03	0.06	0.06	0.02	0.03	0.00	0.01	0.04	0.00	0.03	0.02	0.02	0.05
Ca	0.20	0.05	0.41	0.30	0.03	0.51	0.29	0.03	0.61	0.30	0.02	0.44	0.20	0.04	0.33	0.02	0.00	0.48	0.18	0.01	0.52	0.28	0.00	0.55	0.22	0.01	0.36	0.29	0.11	0.30
Na	0.78	0.96	0.59	0.72	0.91	0.50	0.70	1.00	0.43	0.72	1.00	0.59	0.79	1.00	0.65	0.76	0.97	0.52	0.78	0.94	0.48	0.74	1.02	0.44	0.76	1.04	0.65	0.73	0.90	0.66
Ba	0.00	0.00	0.00	0.00	0.00	0.00	0.00	0.00	0.00	0.00	0.00	0.00	0.00	0.00	0.00	0.00	0.00	0.00	0.00	0.00	0.00	0.00	0.00	0.00	0.00	0.00	0.00	0.00	0.00	0.00
Mg	0.00	0.01	0.00	0.00	0.01	0.00	0.00	0.00	0.00	0.00	0.00	0.00	0.00	0.00	0.00	0.02	0.01	0.00	0.00	0.02	0.00	0.00	0.00	0.01	0.00	0.01	0.00	0.00	0.00	0.00
Fe	0.01	0.01	0.01	0.01	0.02	0.00	0.01	0.00	0.01	0.01	0.01	0.00	0.01	0.00	0.01	0.02	0.01	0.01	0.01	0.04	0.01	0.01	0.00	0.02	0.00	0.01	0.00	0.00	0.00	0.01
∑	1.04	1.03	1.02	1.04	1.02	1.02	1.05	1.04	1.05	1.04	1.04	1.03	1.06	1.04	1.03	0.99	1.03	1.04	1.04	1.07	1.03	1.06	1.03	1.04	1.03	1.07	1.05	1.04	1.04	1.02
x_{kfs}	0.05	0.01	0.01	0.01	0.05	0.01	0.05	0.00	0.00	0.01	0.01	0.00	0.06	0.00	0.03	0.18	0.05	0.03	0.06	0.06	0.02	0.03	0.00	0.01	0.04	0.00	0.03	0.02	0.02	0.05
x_{an}	0.19	0.05	0.41	0.29	0.03	0.50	0.28	0.03	0.58	0.29	0.02	0.43	0.19	0.03	0.33	0.02	0.00	0.47	0.18	0.01	0.51	0.27	0.00	0.55	0.22	0.01	0.35	0.28	0.11	0.30
x_{ab}	0.76	0.95	0.58	0.70	0.92	0.49	0.67	0.96	0.41	0.70	0.97	0.57	0.75	0.96	0.64	0.80	0.95	0.50	0.76	0.93	0.47	0.70	0.99	0.44	0.74	0.99	0.62	0.71	0.87	0.65

Tab. 3a: Representative mica compositions as determined by EMP analyses.

	B2-2		B3-1		B3-3		B4-2	
	untreated	**CO_2-treated**	**untreated**	**CO_2-treated**	**untreated**	**CO_2-treated**	**untreated**	**CO_2-treated**
	Ms	**Bio**	**Ms**	**Bio**	**Ms**	**Ms**	**Ms**	**Ms**
SiO_2	48.10	34.53	46.60	42.52	48.29	46.42	44.59	47.35
Al_2O_3	30.79	13.10	30.51	17.53	30.21	34.01	35.21	31.63
MgO	2.02	8.71	1.64	12.55	1.01	0.60	0.66	1.14
FeO	2.56	23.10	4.41	14.65	4.70	2.89	2.07	3.20
TiO_2	0.42	4.11	0.80	1.75	0.53	0.60	1.05	0.19
MnO	0.04	0.28	0.00	0.18	0.03	0.02	0.01	0.03
CaO	0.09	0.04	0.00	0.14	0.07	0.04	0.01	0.07
BaO	0.27	0.56	0.15	0.19	0.12	0.35	0.09	0.09
Na_2O	0.29	0.51	0.73	0.11	0.32	1.00	0.43	0.25
K_2O	10.99	8.10	10.07	6.78	10.19	9.37	10.73	10.58
F	0.02	1.33	0.00	0.13	0.01	0.03	0.04	0.39
Cl	0.00	0.20	0.00	0.07	0.01	0.00	0.00	0.00
∑	95.58	94.58	94.91	96.58	95.47	95.31	94.87	94.91
normalized to 11 oxygen								
Si	3.23	2.79	3.18	3.05	3.20	3.12	3.02	3.20
Al	0.77	1.21	0.82	0.95	0.80	0.88	0.98	0.80
∑	4.00	4.00	4.00	4.00	4.00	4.00	4.00	4.00
Al	1.67	0.04	1.64	0.53	1.67	1.81	1.83	1.72
Mg	0.20	1.05	0.17	1.34	0.10	0.06	0.07	0.11
Fe	0.14	1.56	0.25	0.88	0.27	0.16	0.12	0.18
Ti	0.02	0.25	0.04	0.09	0.03	0.03	0.05	0.01
Mn	0.00	0.02	0.00	0.01	0.00	0.00	0.00	0.00
∑	2.04	2.92	2.10	2.86	2.08	2.06	2.07	2.02
K	0.94	0.84	0.88	0.62	0.90	0.80	0.93	0.91
Na	0.04	0.08	0.10	0.02	0.04	0.13	0.06	0.03
Ca	0.01	0.00	0.00	0.01	0.01	0.00	0.00	0.00
Ba	0.01	0.02	0.00	0.01	0.00	0.01	0.00	0.00
∑	1.00	0.94	0.98	0.65	0.95	0.94	0.99	0.94

Note: Mineral abbreviations after Kretz (1983)

Tab. 3b: Representative analcime compositions as determined by EMP analyses.

	B2-2		B2-3*	B3-1		B3-3		B4-2°
	untreated	CO_2-treated	CO_2-treated	untreated	CO_2-treated	untreated	CO_2-treated	untreated
SiO_2	61.49	59.77	58.34	60.65	59.18	59.43	59.34	59.73
Al_2O_3	22.57	21.22	22.12	21.90	21.85	22.38	21.60	21.97
MgO	0.00	0.00	0.00	0.00	0.00	0.00	0.00	0.00
FeO	0.03	0.05	0.00	0.05	0.03	0.08	0.03	0.02
TiO_2	0.00	0.01	0.01	0.00	0.00	0.00	0.00	0.00
MnO	0.00	0.02	0.02	0.00	0.04	0.02	0.01	0.00
CaO	0.00	0.00	0.02	0.00	0.01	0.01	0.00	0.00
Na_2O	13.00	13.23	13.83	13.25	13.22	13.44	13.16	13.22
K_2O	0.01	0.02	0.02	0.03	0.00	0.01	0.02	0.01
Cl	0.01	0.00	0.00	0.01	0.01	0.00	0.00	0.00
SO_2	0.00	0.00	0.00	0.00	0.00	0.00	0.01	0.00
∑	97.11	94.33	94.35	95.88	94.33	95.37	94.15	94.95
normalized to 6 oxygen								
Si	2.10	2.11	2.07	2.10	2.09	2.08	2.10	2.09
Al	0.91	0.88	0.92	0.90	0.91	0.92	0.90	0.91
∑	3.01	2.99	2.99	3.00	3.00	3.00	3.00	3.00
Na	0.86	0.91	0.95	0.89	0.91	0.91	0.90	0.90
K	0.00	0.00	0.00	0.00	0.00	0.00	0.00	0.00
Ca	0.00	0.00	0.00	0.00	0.00	0.00	0.00	0.00
∑	0.86	0.91	0.95	0.89	0.91	0.91	0.90	0.90

Note: Mg, Fe, Ti, Mn, Cl and S are all <0.005 after normalization and not listed.

*: no EMP measurement for untreated set B2-3 available

°: no EMP measurement for CO2-treated set B4-2 available

Fischer et al. - Figure 1

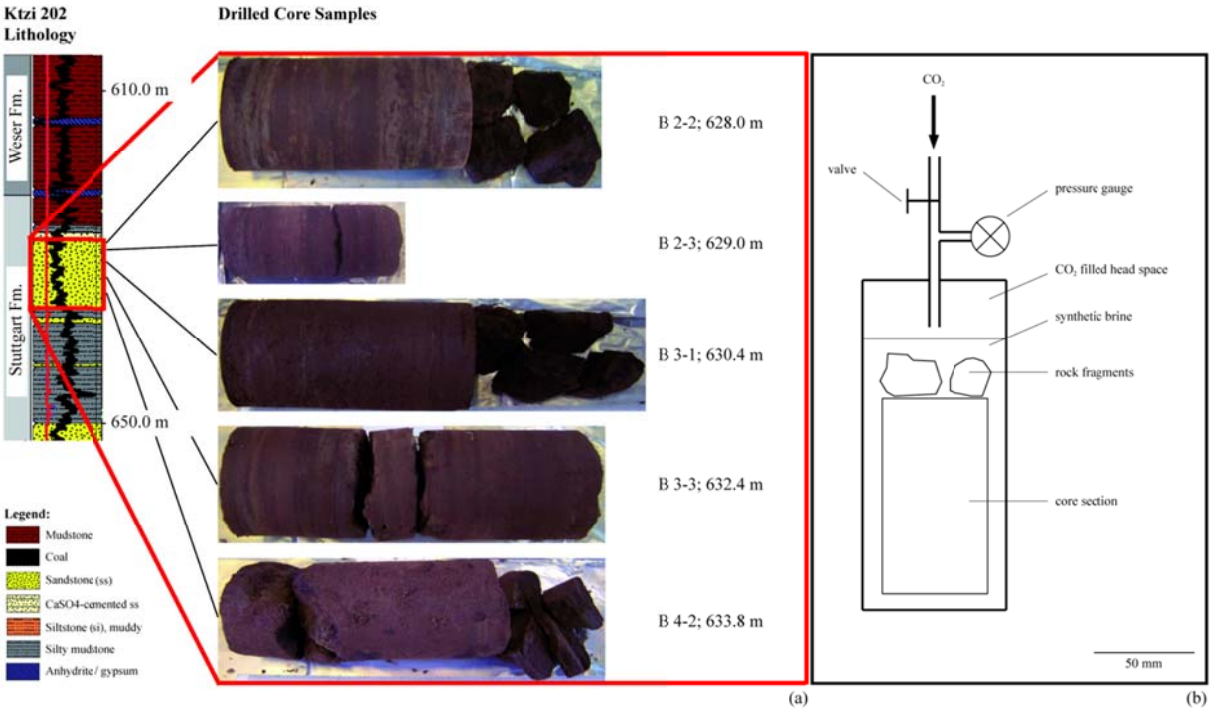

Fischer et al. - Figure 2

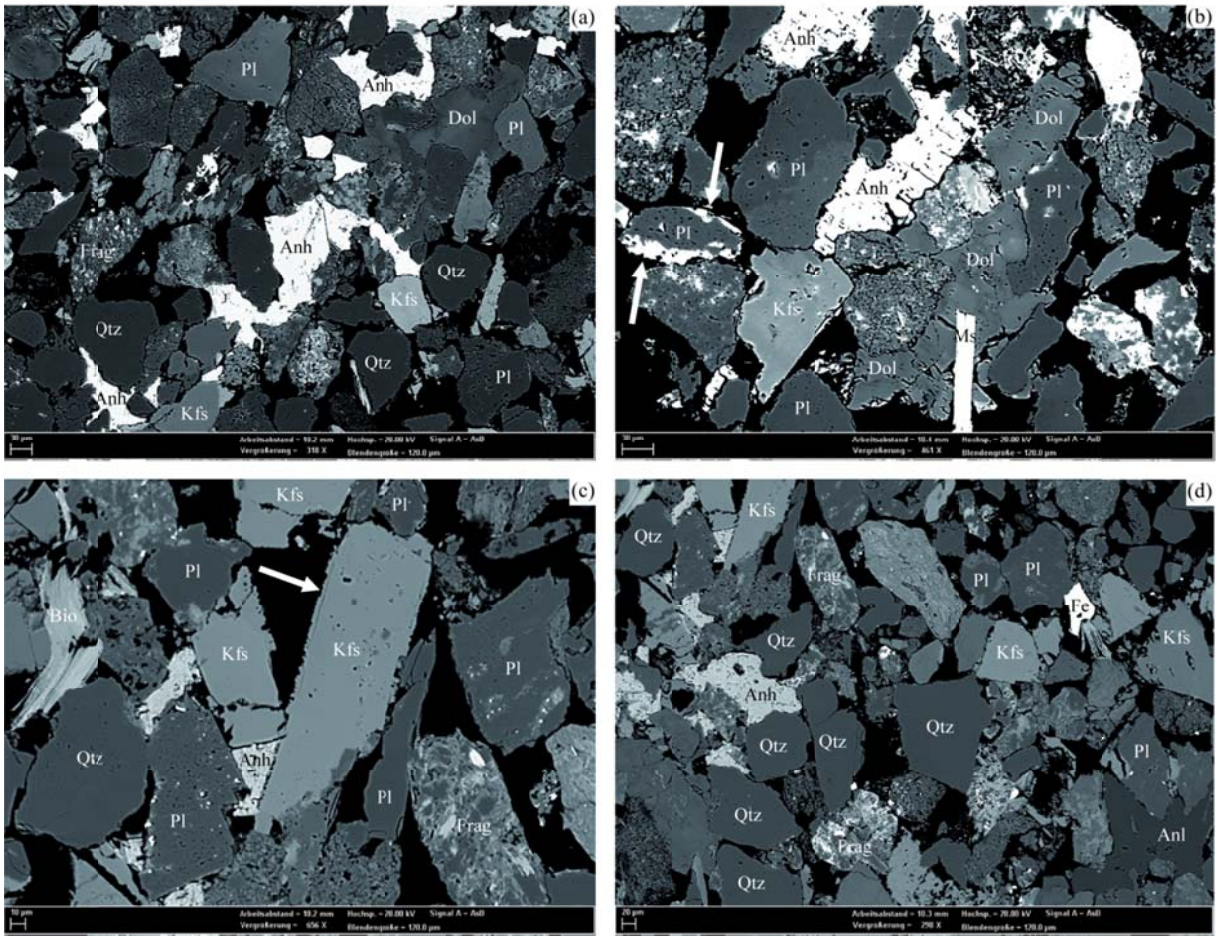

Fischer et al. - Figure 3

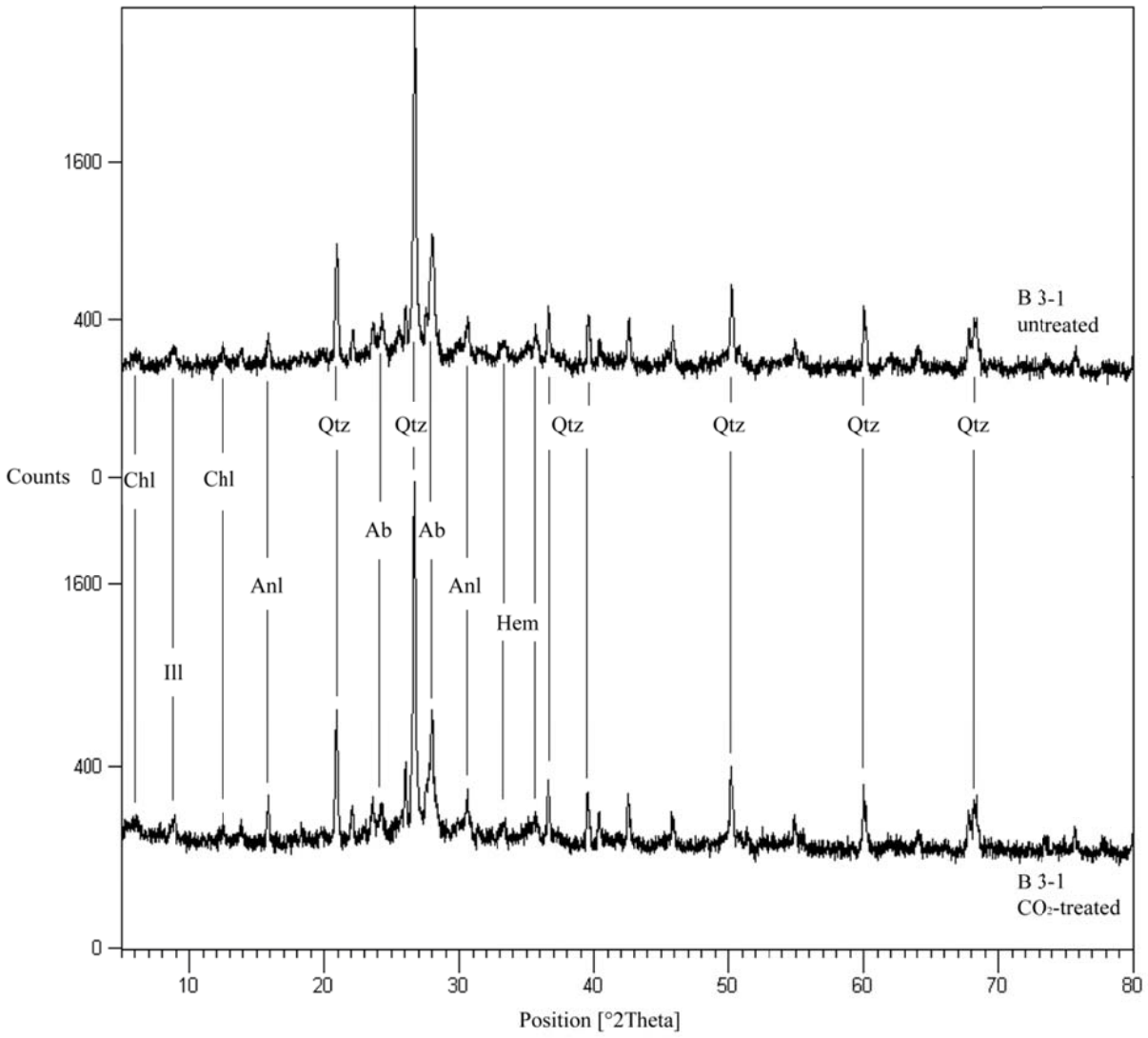

Fischer et al. - Figure 4

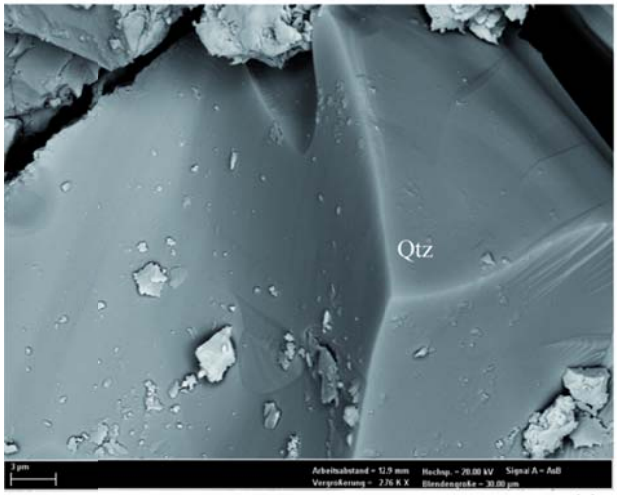

(a)

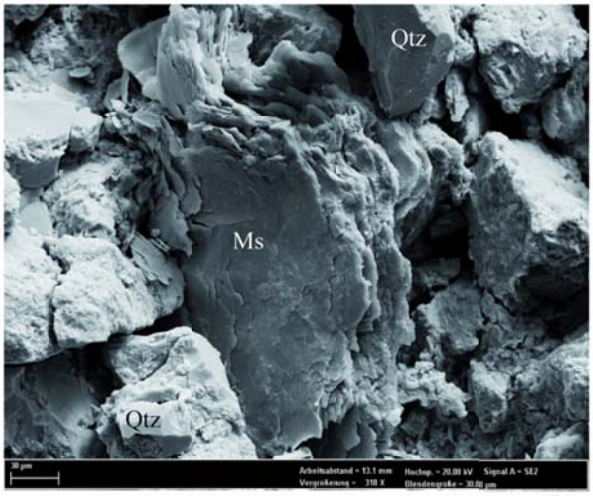

(b)

(c)

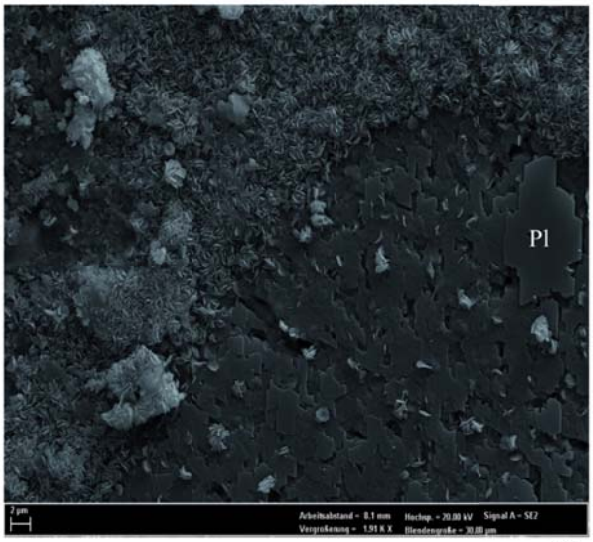

(d)

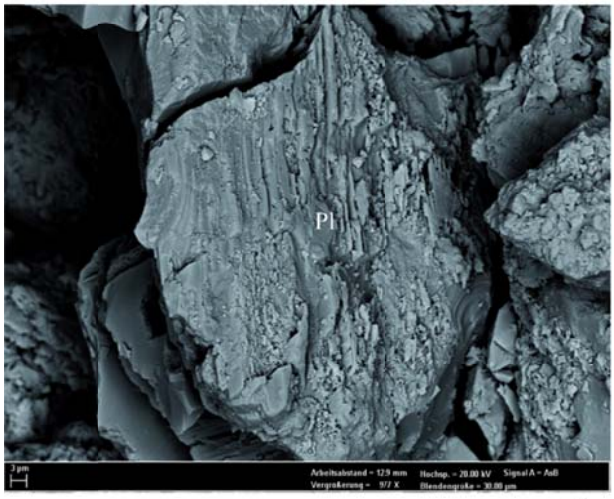

(e)

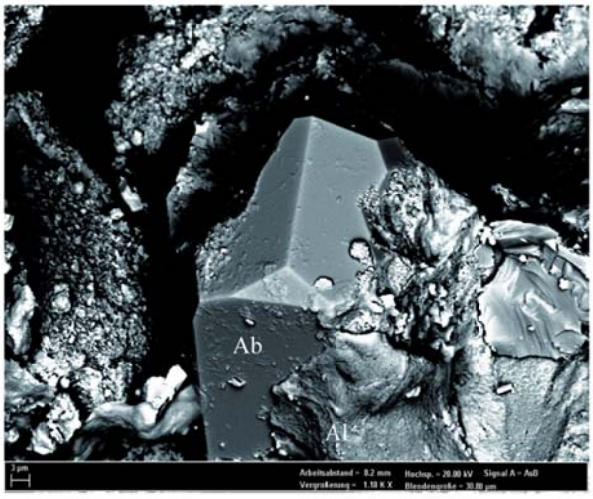

(f)

Fischer et al. - Figure 5